Inhibition of Interactions Between NDPK-B and NDPK-C in Presence of Graphene Oxide

Andrey O. Zaznaev[1#], *Isaac G. Macwan*[1]*

[1]Department of Electrical and Biomedical Engineering, Fairfield University, 1073 N Benson Road, Fairfield CT 06824, USA

KEYWORDS: NDPK, Graphene Oxide, Molecular Dynamics, Heart Failure

ABSTRACT. During a heart failure, higher amount of nucleoside diphosphate kinase (NDPK) enzyme in the sarcolemma membrane inhibits the synthesis of second messenger cyclic adenosine monophosphate (cAMP), which is required for the regulation of the calcium ion balance for normal functioning of the heart. In a dependent pathway, NDPK normally phosphorylates the stimulatory guanosine diphosphate, GDP(s), to a guanosine triphosphate, GTP(s), on the heterotrimeric (α, β and γ subunits) guanine nucleotide binding protein (G protein), resulting in the stimulation of the cAMP formation. In case of a heart failure, an increased quantity of NDPK also reacts with the inhibitory GDP(i), which is converted to a GTP(i), resulting in the inhibition of the cAMP formation. Typically, the βγ dimer of the G protein binds with hexameric NDPK-B/C complex and receives the phosphate at the residue His266 from residue His118 of NDPK-B. It is known that NDPK-C is required for NDPK-B to phosphorylate the G protein. In this work, the interactions between NDPK-B and NDPK-C are quantified in the presence and absence of graphene oxide

(GO) as well as those between NDPK-B and GO through stability analysis involving hydrogen bonds, center of mass (COM), root mean square deviation (RMSD), and salt bridges, and energetics analysis involving van der Waals (VDW) and electrostatic energies. Furthermore, the role of water molecules at the interface of NDPK-B and NDPK-C as well as between NDPK-B and GO is investigated to understand the nature of interactions. It is found that the adsorption of NDPK-B on GO triggers a potential conformational change in the structure of NDPK-B, resulting in a diminished interaction with NDPK-C. This is confirmed through a reduced center of mass (COM) distance between NDPK-B and GO (from 40 Å to 30 Å) and an increased COM distance between NDPK-B and NDPK-C (from 50 Å to 60 Å). Furthermore, this is also supported by fewer salt bridges between NDPK-B and NDPK-C, and an increased number of hydrogen bonds formed by the interfacial water molecules. As NDPK-C is crucial to be complexed with NDPK-B for successful interaction of NDPK-B with the G protein, this finding shows that GO can suppress the interactions between NDPK-B/C and G proteins, thereby providing an additional insight into the role of GO in the heart failure mechanism.

INTRODUCTION. In a recent report, American Heart Association announced that the prevalence of heart failure continues to rise over time, with aging of the population. An estimated 6.2 million American adults ≥20 years of age had heart failure between 2013 and 2016, compared with an estimated 5.7 million between 2009 and 2012[1]. Clearly, this is an ever-growing health concern, and research work regarding heart failure and especially molecular mechanisms underlying it are of increasing importance. Differences in molecular concentrations and activities account for the heart failure. Nucleoside diphosphate kinases (NDPKs) are a family of proteins involved in nucleotide homeostasis and protein histidine kinase[2]. There are four different types of NDPKs – A, B, C, and D. The ones involved with the G protein binding are the NDPK complex, NDPK-B

42 and NDPK-C[3,4]. While similar, NDPK-B is a hexamer of identical chains and NDPK-C is a trimer
43 of identical chains and the latter contains the amino acid tail that the NDPK-B does not have[5,6]. In
44 a non-failing heart, the normal concentration of NDPK complex reacts with G_s (G stimulatory)
45 protein, which causes second messenger cyclic adenosine monophosphate (cAMP) synthesis via
46 the beta-adrenergic pathway. cAMP activates protein kinase A (PKA), which in turn activates the
47 Ca^{2+} channels and maintains calcium homeostasis essential for normal cardiac function[7]. Failing
48 heart, however, is associated with elevated NDPK and Gi (G inhibitory) contents. More NDPK
49 binds with the G_i protein, which causes the suppression of cAMP synthesis and thus lower PKA
50 activation, resulting in an imbalanced calcium ion homeostasis. This leads to heart failure when
51 systolic and/or diastolic functions are limited[8,9]. G proteins (guanine-nucleotide binding proteins)
52 are also a family of proteins that are membrane-bound signal transducers[10]. Two main types of G
53 proteins – stimulatory and inhibitory – share a common heterotrimeric structure (containing α, β,
54 and γ subunits). The α subunit consists of the bound GDP molecule[11]. NDPK-B and in particular
55 its residue Histidine-118 (His118) is involved in substrate channeling of phosphate to residue
56 Histidine-266 (His266) on β subunit of G protein, which then releases Gα from the Gβγ complex,
57 and the GDP on Gα accepts a phosphate from ATP thereby converting to GTP[3]. As a recent study
58 suggests, NDPK-C is essential for the interaction between NDPK complex and G protein[4]. A
59 possible therapeutic strategy against heart failure is to block the interactions between NDPK-BC
60 and G_i protein. As the binding mechanism suggests, some options include blocking the His118
61 residue on NDPK-B or removing NDPK-C from the interaction scene. In this study, the
62 investigated agent presumably capable of reaching these goals is graphene oxide (GO).

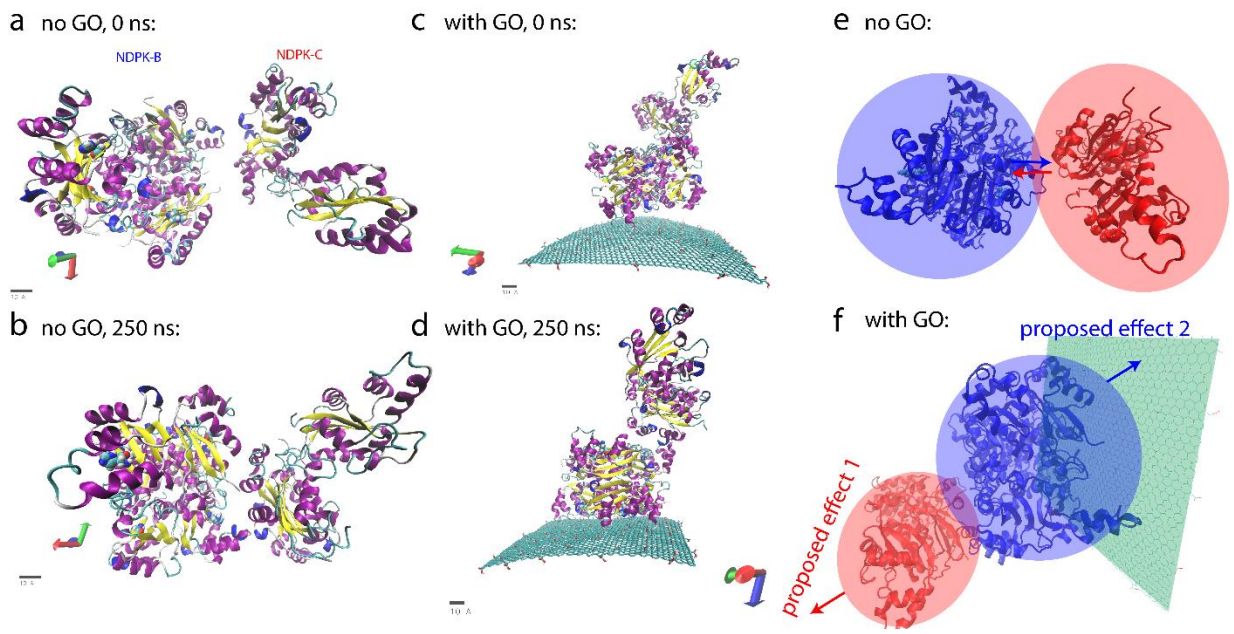

Figure 1. Trajectory screenshots and schemes of simulated systems: (a) — (d) Two systems (with and without GO) at the start (0 ns) and at the finish (250 ns) of the simulations. (e) — (f) Possible changes to the NDPK-BC complex that are hypothesized to occur based on the introduction of GO to the system. "Proposed effect 1" is the NDPK-C moving away from NDPK-B, "Proposed effect 2" is NDPK-B adsorbing on GO.

The choice of this nanomaterial was made because it is water-soluble and non-toxic[12–14]. It has also been shown in a recent article that GO has a potential to suppress the interactions between His118 and G protein by having NDPK-B adsorbed on GO[15].

As NDPK-C proves to be essential for NDPK – G protein interaction whereas NDPK-B is capable of adsorbing on GO, in this article we investigate how GO affects the interactions of NDPK-B and NDPK-C. The existing scientific literature has little information to support the use of nanoparticles to suppress the interactions between NDPK-B and NDPK-C. Our hypothesis is that as NDPK-B adsorbs on GO, NDPK-C does not follow NDPK-B and is disassociated from it. Based on this it is proposed that GO is capable of removing NDPK-C from the interaction scene of NDPK complex

78 and G protein. The objectives of this work are to quantify the molecular events between NDPK-B
79 and NDPK-C in presence of GO and investigate how GO affects the interactions between them.
80 These results are further compared with the control simulations between NDPK-B and NDPK-C
81 in the absence of GO. Figure 1 shows the two systems with and without GO and the potential
82 hypothesis along with the proposed effects based on the adsorption of NDPK-B on GO and its
83 moving away from NDPK-C.

84 **RESULTS AND DISCUSSION.** The trajectories obtained from the 250 ns production runs were
85 analyzed based on the stability of the interacting molecules and energy evaluation of the interface.
86 The first group is stability analysis, which includes root mean square deviation (RMSD), hydrogen
87 bonds, center of mass (COM), salt bridges, and secondary structure analyses. Stability analysis
88 typically determines how stable a molecule is within the timeframe of the simulation and its
89 tendency to deviate, highlighting possible factors, both internal and external, influencing its
90 behavior. The second group of analyses determined the various non-bonding energies of the
91 molecules and is used to investigate the molecular adsorption tendencies evident from changes in
92 energies. This group includes determining Van der Waals energies (between molecules) and
93 electrostatic energies (both within and between molecules). Furthermore, analyses involving the
94 optimal distance between NDPK-B and NDPK-C and between NDPK-B and GO were performed
95 along with the role of interfacial water molecules during such interactions. We assign the time
96 from the beginning of the simulation to ~140 ns as pre-interaction and from ~140 ns onwards as
97 post-interaction.
98 As shown in Figures 2a and 2b, after 125ns, in the absence of GO, NDPK-B has a deviation of ~2
99 Å whereas NDPK-C deviate by ~3.75 Å. In contrast to this, in the presence of GO, NDPK-B
100 deviates by ~4 Å while NDPK-C shows a deviation of ~3.6 Å indicating that NDPK-B underwent

101 significant conformational changes owing to its adsorption onto GO whereas NDPK-C started to
102 lose its interaction with NDPK-B. From Figure 2c, the deviation of ~2.5 Å before ~140 ns is
103 indicative of the pre-interaction phase during which the interactions between NDPK-B and GO
104 started to increase whereas from ~140ns onwards, there is an increase in the deviation of GO to
105 ~3 Å, which indicates the post-interaction period during which not only the interactions between
106 NDPK-B and GO became stronger but more importantly those between NDPK-B and NDPK-C
107 would have started to diminish. These time checkpoints provide the preliminary time division of
108 the pre- and post-interactions. The adsorption of NDPK-B onto GO and the eventual diminishing
109 of the interactions between NDPK-B and NDPK-C is further verified by analyzing the energy of
110 interaction between these molecules.

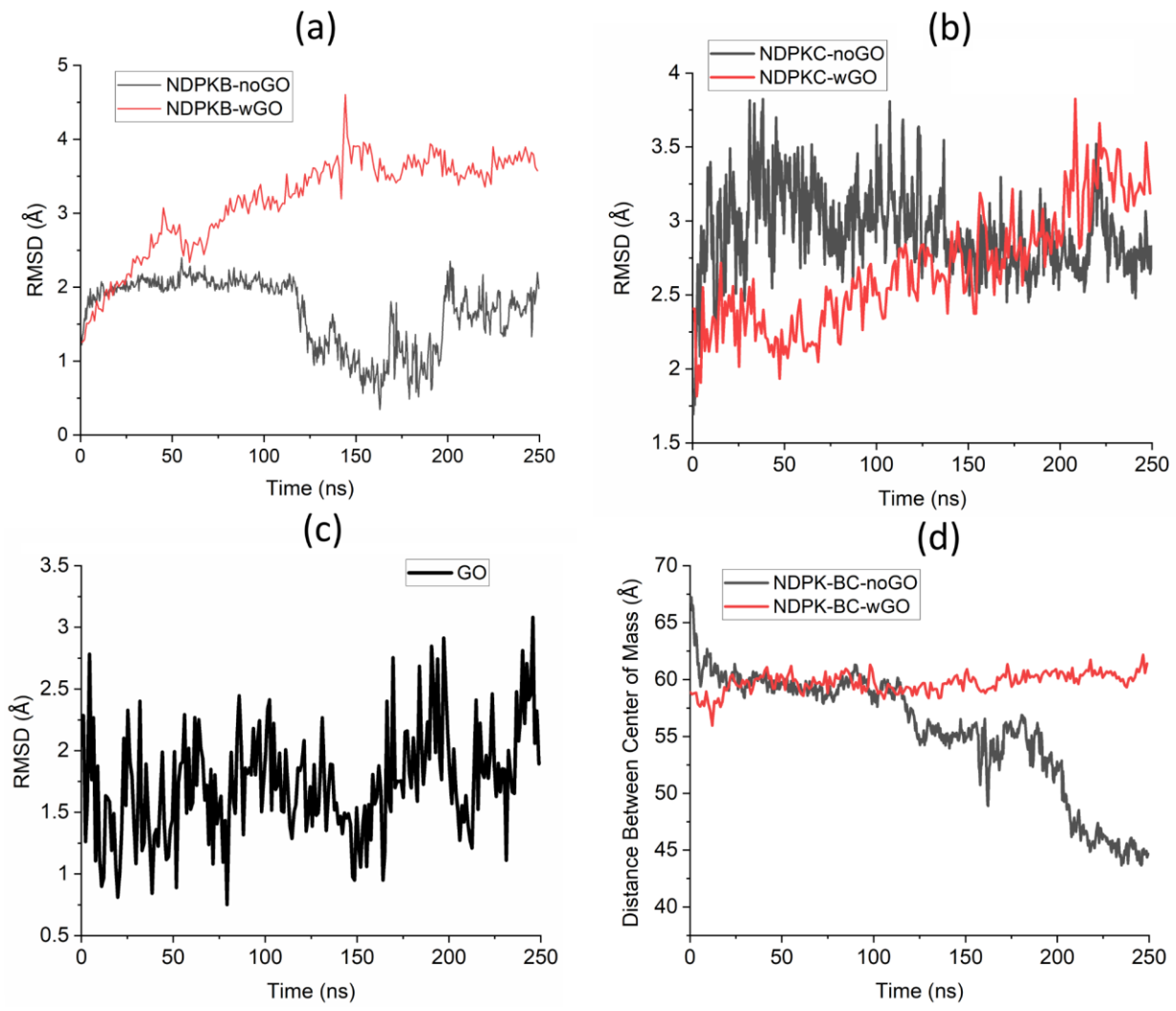

Figure 2. Stability Analysis of NDPK-B, NDPK-C in the presence and absence of graphene oxide. (a) RMSD of NDPK-B. (b) RMSD of NDPK-C. (c) RMSD of GO. (d) Distance between the center of masses (COM) of NDPK-B and NDPK-C. In all plots, noGO – no (absence of) GO; wGO – with (presence of) GO.

COM analysis utilizing the TCL scripts was used to investigate how distance between molecular centers of masses changes with respect to time, i.e., if different pairs of molecules move towards or away from each other. Figure 2d shows the COM distance between NDPK-B and NDPK-C in the presence and absence of GO and it is found that COM distance decreases to ~55 Å starting at

120 ~115 ns and further decreases to ~43 Å beyond 200ns in the absence of GO, indicating that they
121 come closer to each other as time goes by. On the contrary, when GO is present, initially, NDPK-
122 B and NDPK-C do not change their positions relative to each other, whereas after ~20 ns, there is
123 a jump in the COM data from 57 Å to 60 Å. This is supported by the first milestone in the
124 interactions in the presence of GO, where at ~50 ns, the interactions between NDPK-B and GO
125 started to stabilize. Similarly, at ~150 ns and onwards, there is an increasing trend in the COM
126 between NDPK-B and NDPK-C again supporting the second milestone when NDPK-B and
127 NDPK-C started to lose interactions with each other. This finding indicates that the presence of
128 GO refrains NDPK-B and NDPK-C from coming closer to each other. This may be interpreted as
129 a possible way to block the interactions between these proteins.
130 Figure 3a shows that the distance between the center of masses of NDPK-B and GO decreases
131 rapidly during the first 25 ns, clearly showing the two milestones at ~50 ns and ~150 ns, after
132 which the distance between NDPK-B and GO reduces further, finally settling at ~30 Å, indicating
133 an increase in the affinity interactions between NDPK-B and GO. Hydrogen bonds analysis was
134 utilized to further confirm the stability of individual molecules and that of the interface between
135 the molecules by quantifying the strength of interactions between them. A donor – acceptor
136 distance of 3 Å and the angle cut-off of 20 degrees is used as the criteria for the hydrogen bonds
137 analysis. It is important to note that the hydrogen bond analysis do not include the salt bridges,
138 which are analyzed separately. From Figure 3b, we can see that both in presence and absence of
139 GO, the hydrogen bonds between NDPK-B and NDPK-C rapidly increase during the first 50 ns,
140 then maintaining relatively stable values (though in the presence of GO, the average number is
141 slightly larger). At around 200 ns, however, the number of hydrogen bonds starts to differ based
142 on whether GO is present or not. In the presence of GO, the number of hydrogen bonds start to

drop in comparison to the absence of GO, in which case, the hydrogen bonds rise substantially. This supports the proposed hypothesis that in the presence of GO NDPK-B and NDPK-C would experience diminished interactions. Non-bonding interaction energy analysis through Van der Waals (VDW) and electrostatic energies between NDPK-B and NDPK-C was done to understand the interactions at the interface. Figures 3c and 3d show the VDW interactions between NDPK-B and NDPK-C in the presence and absence of GO as well as those between NDPK-B and GO.

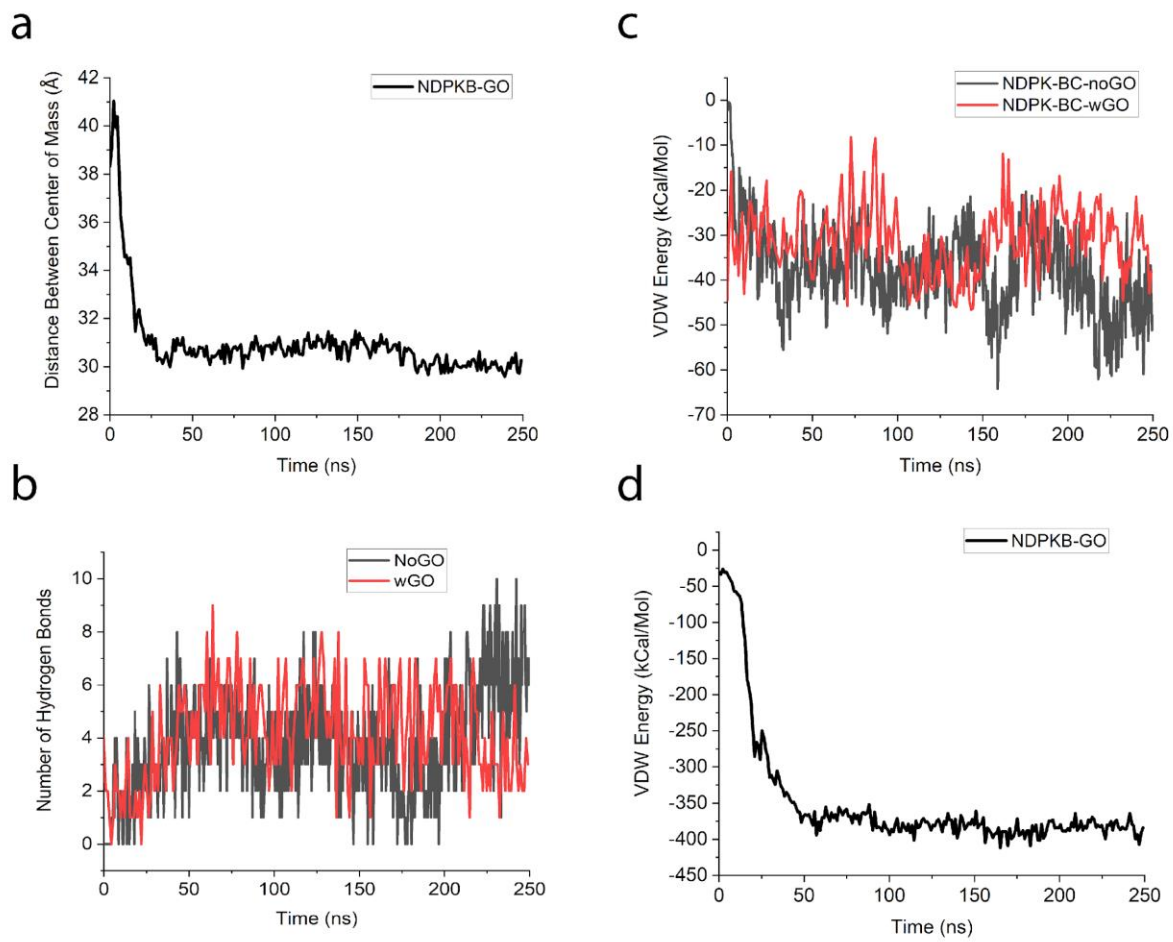

Figure 3. Stability and energetics analysis between NDPK-B, NDPK-C and graphene oxide. (a) Distance between the center of mass (COM) between NDPK-B and GO. (b) Number of hydrogen bonds between NDPK-B and NDPK-C in the presence and absence of GO. (c) Van-der-Waals

(VDW) energy between NDPK-B and NDPK-C in the presence and absence of GO. (d) VDW energy between NDPK-B and GO.

It is found that in the presence of GO, the VDW energy between NDPK-B and NDPK-C is comparable to that in the absence of GO, correctly pointing out that VDW energy is dominant largely in case of surface adsorption as evident from Figure 3d. As it can be seen from Figure 3d, the VDW energy between NDPK-B and GO is ~375 kCal/Mol at 50ns and after 150 ns, there is ~25 kcal/mol increase in the energy indicating that after 150 ns, NDPK-B started to lose its interactions with NDPK-C and got adsorbed on GO with larger energy.

As NDPK-B and NDPK-C interacts with each other, they would also form salt bridges to maintain the stable interactions. Table 1 shows the analysis of such intermolecular salt bridges between NDPK-B and NDPK-C. As we can see, there are 12 salt bridges that are formed (< 4 Å distance between the interacting residues) between NDPK-B and NDPK-C throughout the course of the simulation in the absence of GO, while only two are formed in the presence of GO. In addition, four weak salt bridges (distance of 4 Å to 5 Å between the interacting residues) were detected without GO while only two such weak salt bridges were seen in the presence of GO. Detailed plots of all the salt bridges in the presence and absence of GO are included in the supplementary section figures S5 to S10. These two pieces of data combined imply that in the presence of GO, salt bridge formation between NDPK-B and NDPK-C is inhibited.

176 **Table 1.** Intermolecular salt bridges between NDPK-B and NDPK-C

Salt bridge type	Without GO	With GO
Formed	12 ASP138—LYS49, ASP57—ARG152, ASP57—ARG73, GLU141—LYS128, GLU46—ARG105, GLU5—ARG73, GLU67—LYS56, GLU71—LYS49, GLU74—LYS66, GLU63—LYS85, GLU62—LYS85, GLU152—ARG145	2 GLU152—ARG145, GLU62—LYS85
Weak	4 ASP121—LYS83, ASP57—ARG145, GLU46—ARG102, ASP54—ARG152	2 ASP54—ARG152, GLU74—LYS124
Broken	3 GLU74—LYS124, GLU141—LYS49, GLU141—LYS56	3 GLU5—ARG73, GLU63—LYS85, ASP57—ARG152

177

178 Another aspect of interaction energy is based on electrostatic charges, which together with VDW
179 energy quantifies the overall (total) interaction energy. Figure 4a shows electrostatic energy within
180 NDPK-B, which is found to be more negative (attractive) in the presence of GO, starting 140 ns
181 (post-interaction period). Similarly, for NDPK-C, in Figure 4b, it is found that the electrostatic
182 energy is higher (more negative values) in the absence of GO, especially after 150ns. Interestingly,
183 it is found that beyond 200ns, the overall electrostatic energy within NDPK-C in the presence of
184 GO is very close to the absence of GO indicating that it regains its conformational structure once
185 NDPK-B moves away. Together, these results indicate that the conformational energy landscapes
186 for NDPK-B and NDPK-C are contrary to each other when it comes to adsorption. As can be seen,
187 in the absence of GO, when NDPK-B interacts well with NDPK-C, it undergoes a sudden decrease
188 (repulsion) in its conformational energy (Figure 4a) whereas NDPK-C undergoes a sudden
189 increase (attraction) in its conformational energy (Figure 4b). This behavior related to the

conformational energy is preserved in the presence of GO, where NDPK-B shows a decrease (repulsion) in its conformational energy but to a lesser extent due to its adsorption on GO.

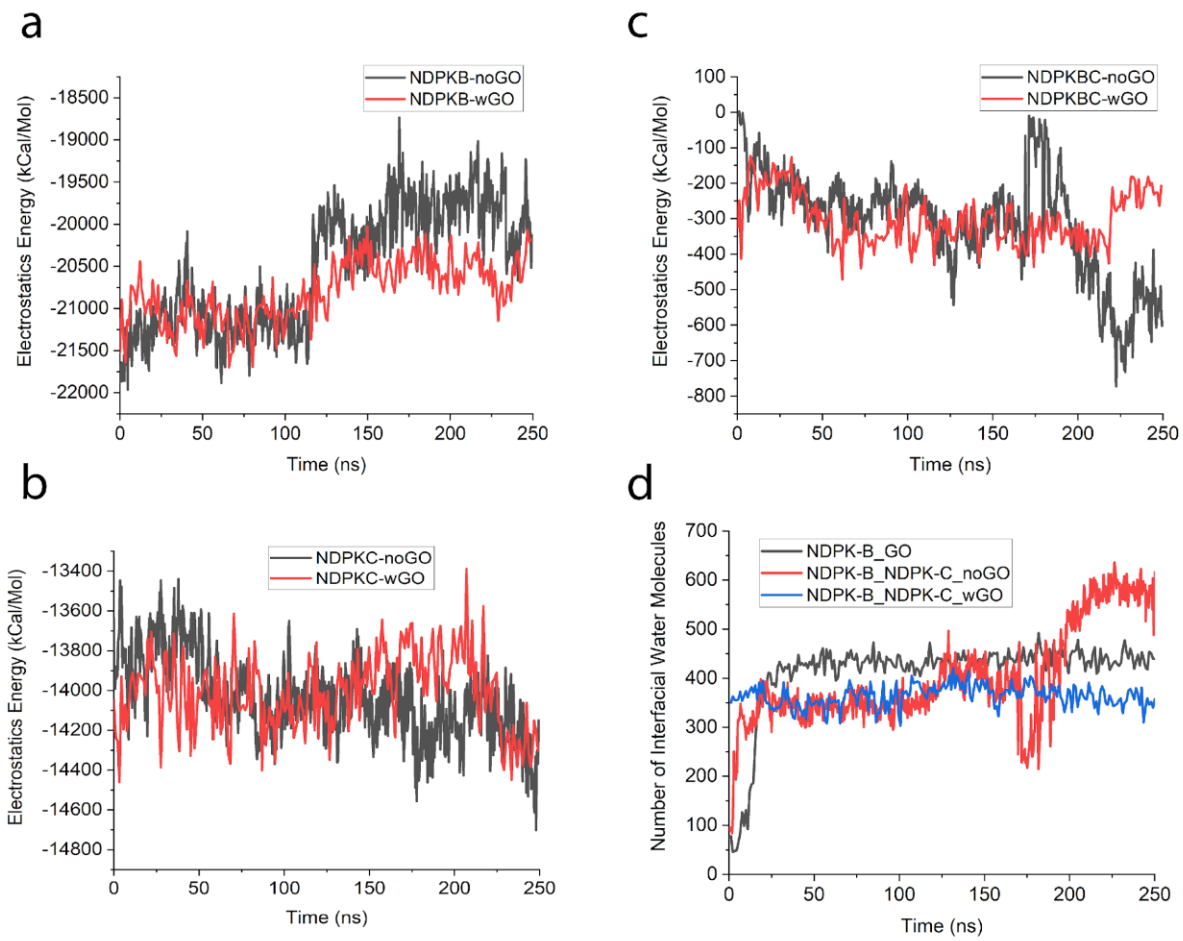

Figure 4. Electrostatics energy and role of interfacial water molecules. (a) Electrostatics energy within NDPK-B in the presence and absence of GO. (b) Electrostatics energy within NDPK-C in the presence and absence of GO. (c) Electrostatics energy between NDPK-B and NDPK-C in the presence and absence of GO. (d) Number of interfacial water molecules between NDPK-B and GO, and between NPDK-B and NDPK-C in the presence and absence of GO.

It is observed that this decrease in the electrostatic energy of NDPK-B in the presence of GO is because it interacts dominantly via the VDW energy with GO. Similar behavior is seen in NDPK-C where it shows a decrease in its conformational energy as it starts to lose its interactions with

201 NDPK-B. Thus, it is found that in the event of adsorption, NDPK-B has a repulsive electrostatic
202 effect whereas NDPK-C has an attractive electrostatic effect. Finally, comparing the electrostatic
203 energy between NDPK-B and NDPK-C (Figure 4c), we find that in the absence of GO, both
204 NDPK-B and NDPK-C are electrostatically bound by up to ~750 kcal/mol. Comparing this to the
205 presence of GO, it is found that the maximum electrostatic energy between the two is at the most
206 ~400 kcal/mol, which reduces further after 200 ns indicating that the interactions between NDPK-
207 B and NDPK-C diminished significantly after 200ns.
208 To understand the interactions at the interface and the nature of the interface, both in the presence
209 and absence of GO, a detailed analysis on the interfacial water molecules, their hydrogen bonds
210 and RMSD was performed along with the optimal distance between the interacting molecules
211 (NDPK-B and NDPK-C as well as NDPK-B and GO). As can be seen from Figure 4d, the number
212 of interfacial water molecules between NDPK-B-GO complex as well as NDPK-B-NDPK-C
213 complex are very different, where the number of interfacial water molecules (~450) in case of
214 NDPK-B-GO complex is stable compared to those between NDPK-B-NDPK-C complex in the
215 absence of GO, where the number of interfacial water molecules increases to ~600, especially after
216 200 ns (when interactions between NDPK-B and NDPK-C were stabilized). Figure 4d also shows
217 that the number of water molecules at the interface of NDPK-B and GO increased sharply at 25
218 ns, when NDPK-B started to interact with GO, in the pre-interaction time and is then maintained
219 at a relatively constant value. In contrast to this, the number of water molecules between NDPK-
220 B and NDPK-C in the presence of GO were maintained at ~375 indicating the inhibiting role of
221 GO to the interactions between NDPK-B and NDPK-C. This also further clarifies the role of
222 interfacial water molecules in forming the complexes via hydrogen bonds. As can be seen from
223 figures 5a and 5b, with a RMSD deviation of ~5 Å, the interfacial water molecules maintained on

an average ~150 hydrogen bonds owing to the increased interactions between NDPK- B and GO starting at 25 ns.

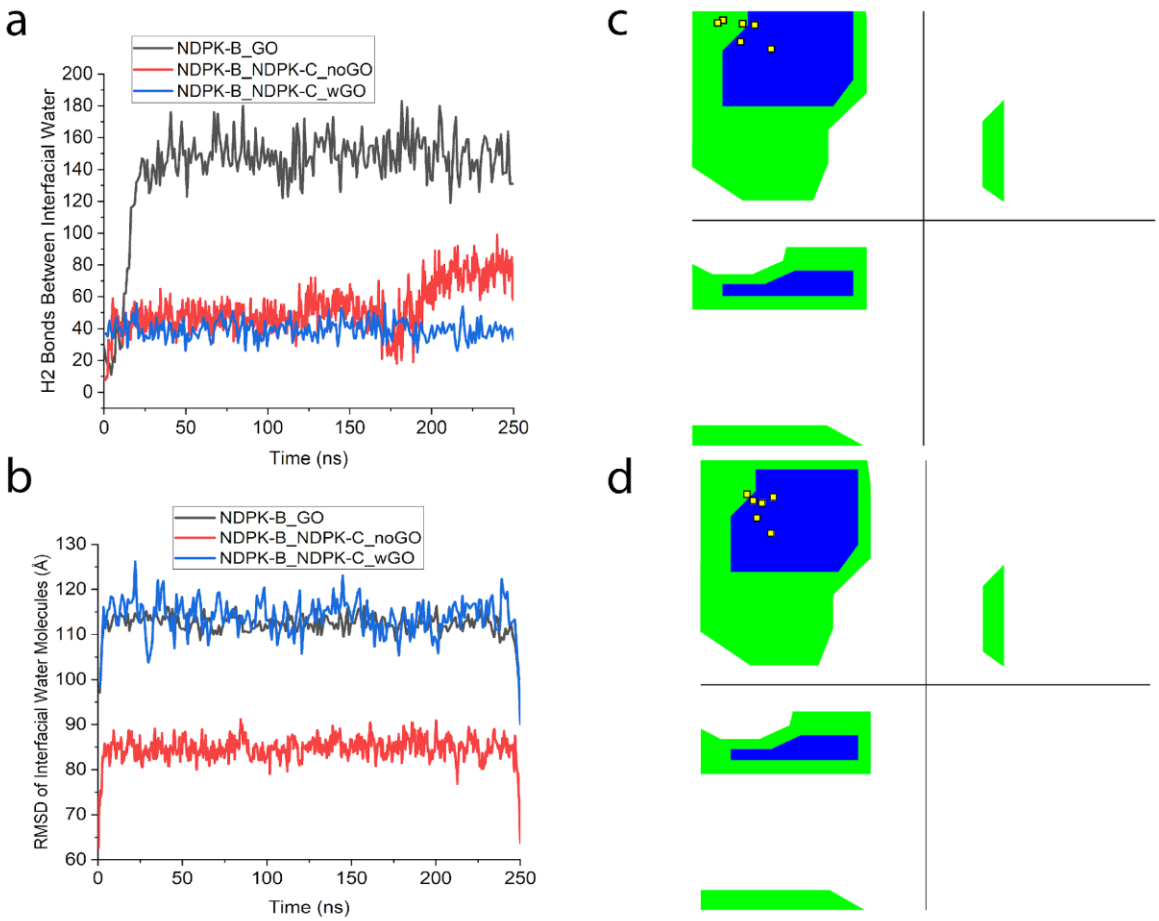

Figure 5. Regulation of interface between NDPK-B and NDPK-C by interfacial water molecules and Ramachandran plots. (a) Hydrogen bonds of the interfacial water molecules at the interface of NDPK-B and GO and between NPDK-B and NDPK-C in the presence and absence of GO. (b) RMSD of the interfacial water molecules between NDPK-B and GO, and between NDPK-B and NDPK-C in the presence and absence of GO. (c) – (d) Ramachandran plots for the six His118 residues in the absence and presence of GO.

A very different situation existed at the interface of NDPK-B and NDPK-C where comparing the presence and absence of GO, we find that in the absence of GO, the number of hydrogen bonds

235 were found to be ~50 until 200 ns and ~80 after 200 ns when the interactions between NDPK-B
236 and NDPK-C were stabilized with RMSD of ~8 Å, whereas in the presence of GO, the number of
237 hydrogen bonds between NDPK-B and NDPK-C reduced to ~40 with an increased RMSD of ~15
238 Å. This analysis demonstrates that the presence of interfacial water molecules gives rise to better
239 interactions at the interface with more water molecules present for stable interactions giving rise
240 to more hydrogen bonds. Figures 5c and 5d present an additional layer of analyses of protein
241 structures — the Ramachandran plots. They show the dihedral angles around alpha carbon atoms
242 for the six His118 residues of NDPK-B in the absence (Figure 5c) and presence (Figure 5d) of GO.
243 It is found that in the absence of GO, three of the six residues are in the blue (core) beta sheet
244 region. Conversely, in the presence of GO, five of the six residues are in the blue region indicating
245 that GO can influence the secondary structure around His118 residues. This finding is supported
246 by the secondary structure analysis presented in the supplementary figure S4, where it is found
247 that the residue His118 (part of the beta-sheet) undergoes significant conformational change in the
248 presence of GO.
249 To determine the optimum distance between the interacting molecules, number of atoms and
250 interaction energies were considered for the two complexes involving NDPK-B-NDPK-C as well
251 as NPDK-B-GO. Furthermore, the effect of GO on NDPK-B-NDPK-C complex was also
252 determined by comparing the optimum distance measurements in the presence and absence of GO.
253 Figure 6 represents the first group of exhaustive analyses performed, aiming at finding the
254 optimum distance between NDPK-B and GO. For both figures 6 and 7, a comparison was done
255 with and without hydrogen atoms to understand the interactions between heavy atoms (oxygen,
256 carbon, and nitrogen) as the heavy atoms are more stable and it was also useful to explore the
257 effects of these heavy atoms on the interface.

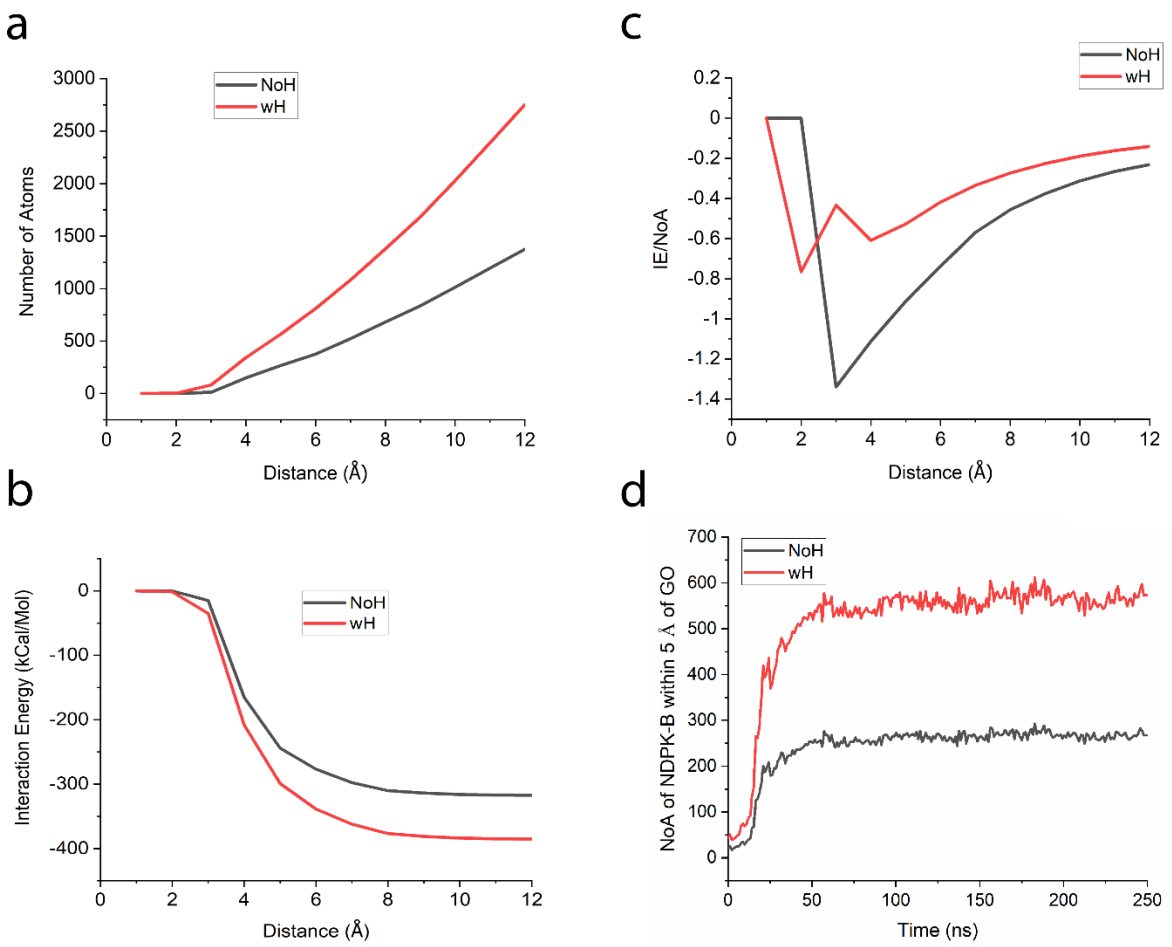

Figure 6. Optimal distance analysis between NDPK-B and GO. (a) Number of atoms between NDPK-B and GO as a function of distance with and without hydrogen atoms. (b) Total interaction energy between NDPK-B and GO as a function of distance with and without hydrogen atoms. (c) Maximum interaction energy per atom between NDPK-B and GO as a function of distance with and without hydrogen atoms. (d) Number of atoms (NoA) of NDPK-B within 5 Å of GO as a function of time with and without hydrogen atoms.

All the values were collected from the time the system became stabilized at ~50 ns. This timestamp was obtained by looking at the stability from the RMSD plot. Figure 6a shows how the number of atoms of NDPK-B (average number with and without hydrogen atoms) is increasing as the distance from the surface of GO was increased from 1 Å to 12 Å (non-bonding cut-off limit). This is not

surprising as we continue to increase the distance from GO, we anticipate encountering more NDPK-B atoms owing to an increase in the radius of our spherical "search spotlight". Similarly, in Figure 6b, the values of the interaction energy, IE (non-bonding energies as a sum of VDW and electrostatic energies), of NDPK-B atoms are decreasing as the spherical "search spotlight" radius centered at GO is increasing from 1 Å to 12 Å. As more NDPK-B atoms are included in the spherical selection zone, we find that beyond ~8 Å, the interactions energy flattens out indicating that there are ~600 heavy atoms (without hydrogen) that play a crucial role in maintaining the interface between NPDK-B and GO. Finally, to determine the optimal distance between NDPK-B and GO, interaction energy per atom is determined as a ratio of IE/NoA for the respective distances (Figure 6c). The negative peak indicates the optimal adsorption distance between NDPK-B and GO of ~3 Å. This further also indicates that ~600 atoms of NDPK-B adsorbed on the surface of GO are enough to maintain the stability of the interface. Figure 6d illustrates a more in-depth look at the number of atoms of NDPK-B within 5 Å of GO throughout the whole course of the simulation. It shows that the number of atoms increased over a period, and after stabilization was achieved, maintained a relatively constant value of ~275 (without hydrogen) and ~575 (with hydrogen) atoms. This also adds an additional lens to show that NDPK-B and GO interacted favorably starting ~50ns and maintained a consistent number of atoms within the adsorption limits. On similar lines, Figure 7 represents exhaustive analysis performed on the interface between NDPK-B and NDPK-C to understand and compare the nature of this interface to that of NDPK-B-GO. Figure 7a shows a comparison between the number of atoms of NDPK-B at certain distances from NDPK-C in the presence and absence of GO. It is found that the number of atoms in the presence and absence of GO, though slightly more in the absence of GO, are very similar.

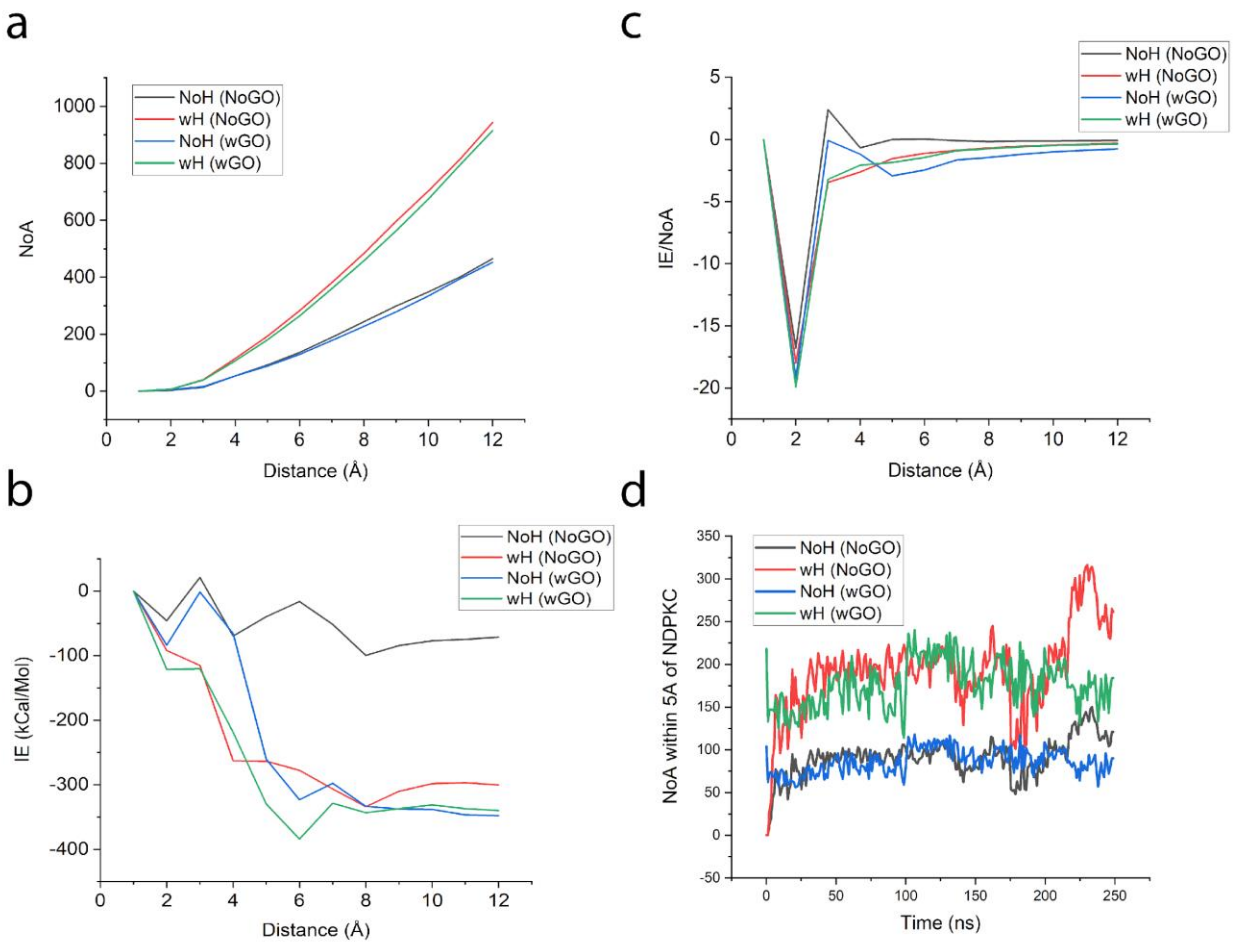

Figure 7. Optimal distance analysis between NDPK-B and NDPK-C. (a) Number of atoms between NDPK-B and NDPK-C as a function of distance in the presence and absence of GO with and without hydrogen atoms. (b) Interaction energy between NDPK-B and NDPK-C as a function of distance in the presence and absence of GO with and without hydrogen atoms. (c) Maximum interaction energy per atom between NDPK-B and NDPK-C in the presence and absence of GO with and without hydrogen atoms. (d) Number of atoms (NoA) of NDPK-B within 5 Å of NDPK-C with respect to time in the presence and absence of GO with and without hydrogen atoms.

For the determination of optimal distance between NDPK-B and NDPK-C, as can be seen from Figures 7b and 7c, it is 2 Å regardless of the presence or absence of GO, which is less than the optimal distance between NDPK-B and GO pointing out the differences in the interactions between

302 the adsorption of NDPK-B on GO, which is largely due to the non-binding energies such as Van
303 der Waals, whereas that between NDPK-B and NDPK-C is largely due to electrostatic interactions.
304 Finally, over a period of 250 ns, the number of atoms of NDPK-B within 5 Å of NDPK-C in the
305 presence and absence of GO shows the dynamics of the interface between NDPK-B and NDPK-C
306 as shown in Figure 7d providing important insights into the early onset of binding between NDPK-
307 B and NDPK-C, after 200 ns, in the absence of GO as can be seen from the comparison between
308 heavy atoms (NoH, NoGO) and (NoH, wGO) plots.

309 **MATERIALS AND METHODS.** The two systems (NDPK-BC alone and NDPK-BC with GO)
310 were first modeled in Visual Molecular Dynamics (VMD)[16], a software used to display and analyze
311 biomolecular systems. The PDB files for NDPK-B and NDPK-C were obtained from Protein Data
312 Bank[17] (codes 1NUE and 1ZS6, respectively)[5], which were then used to generate the protein
313 structure files (PSF) using the CHARMM (Chemistry at HARvard Macromolecular Mechanics)
314 force field parameter files[18]. GO was created using the Molefacture plugin in VMD from the
315 graphene sheet generated using an inbuilt graphene sheet builder plugin, which was then used to
316 create the GO flake of size 96 Å × 90 Å. The chemical structure of the flakes used is
317 C10O1(OH)1(COOH)0.5, also known as OGO[19]. To merge GO with NDPK-BC to set up the
318 second combined system, TCL scripts for moving and rotation of GO were employed. GO was
319 intentionally placed on one side of NDPK-B (~10 Å from its active sites, His118), with NDPK-C
320 on the other side of NDPK-B to minimize the concomitant interactions between NDPK-C and GO.
321 The systems were solvated using the Transferable Intermolecular Potential with 3 Points (TIP3P)
322 water model[20] using the built-in Solvate plugin in VMD. The resulting water box was set up so
323 that each box edge was 10 Å away from the nearest atom. Solvated system was neutralized with
324 NaCl to compensate for the overall net charge in the system, resulting in a total of ~134,000 atoms

325 for the NDPK-BC system and ~382,000 atoms for the NDPK-BC+GO combined system. All
326 simulations were carried out using Nanoscale Molecular Dynamics (NAMD)[21] on an Intel Core i9
327 cluster with a total of 36 cores, and NVIDIA GeForce RTX 2080 GPU. The temperature was
328 maintained at 310 K by the Langevin Thermostat and the pressure was set to 1 atm using Nose-
329 Hoover Langevin-piston barostat with a period of 100 ps and a decay rate of 50 ps. A cut-off of
330 10–12 Å was used for short-range forces and particle mesh Ewald algorithm was used for
331 calculating long-range forces with a time step of 2 fs. A 5000-step energy minimization was
332 performed first to reach a minimum for the potential energy followed by an equilibration of
333 500,000 steps (1 ns). Production runs were performed for 250 ns for each simulation. Analysis of
334 the generated molecular trajectories was primarily conducted in VMD, with the help of TCL and
335 MATLAB scripts. Trajectory analysis was performed using VMD plugins for hydrogen bonds,
336 RMSD, non-bonding and conformational energies, Ramachandran Plot, and salt bridges, as well
337 as the external TCL scripts to analyze distance between center of mass (COM) and number of
338 atoms (NoA). Salt bridges data was further analyzed using a MATLAB script, with cutoff distance
339 of 4 Å.

340 **CONCLUSION.** In this work, the behavior of NDPK-B/C complex was assessed in the absence
341 and presence of GO. It was found that GO causes NDPK-B to adsorb, change conformation, and
342 thus lose interactions with NDPK-C. This was observed through a reduced COM distance between
343 NDPK-B and GO (from 40 Å to 30 Å) and increasing COM distance (from 50 Å to 60 Å) between
344 NDPK-B and NDPK-C. Furthermore, with an optimal distance of 2 Å, the interactions between
345 NDPK-B and NDPK-C were found to be largely governed by electrostatic energies (300 kcal/mol)
346 whereas those between NDPK-B and GO were found to be largely governed by Van der Waals
347 energies (375 kcal/mol) as evident from the optimal distance of 3 Å. It was also found that the

348 number of water molecules at the interface of NDPK-B and GO (~425 molecules) as well as
349 NDPK-B and NDPK-C (~600 molecules in the absence of GO and ~375 molecules in the presence
350 of GO) played a crucial role for the adsorption and that the water molecules formed increased
351 hydrogen bonds only in the presence of favorable interactions at the interface. Diminished
352 interactions within the NDPK-B/C complex can reduce its ability to phosphorylate GDP(i),
353 therefore GO can have an impact of diminishing NDPK-B/C activity in the pathways inhibiting
354 the cAMP formation.
355

356 **REFERENCES**

357 (1) Virani, S. S.; Alonso, A.; Benjamin, E. J.; Bittencourt, M.; Callaway, C. W.; Carson, A. P.;
358 Chamberlain, A. M.; Chang, A. R.; Cheng, S.; Delling, F. N.; Djousse, L.; Elkind, M. S. V.;
359 Ferguson, J. F.; Fornage, M.; Khan, S. S.; Kissela, B. M.; Knutson, K. L.; Kwan, T. W.;
360 Lackland, D. T.; Lewis, T. T.; Lichtman, J. H.; Longenecker, C.; Loop, M. S.; Lutsey, P.
361 L.; Martin, S. S.; Matsushita, K.; Moran, A. E.; Mussolino, M. E.; Perak, A. M.; Rosamond,
362 W. D.; Roth, G. A.; Sampson, U. K. A.; Satou, G. M.; Schroeder, E. B.; Shah, S. H.; Shay,
363 C. M.; Spartano, N. L.; Stokes, A.; Tirschwell, D. L.; VanWagner, L. B.; Tsao, C. W. *Heart*
364 *Disease and Stroke Statistics-2020 Update*; 2020.
365 (2) Attwood, P. V.; Wieland, T. Nucleoside Diphosphate Kinase as Protein Histidine Kinase.
366 *Naunyn-Schmiedeberg's Archives of Pharmacology*. 2015. https://doi.org/10.1007/s00210-
367 014-1003-3.
368 (3) Wieland, T. Interaction of Nucleoside Diphosphate Kinase B with Heterotrimeric G Protein
369 Bγ Dimers: Consequences on G Protein Activation and Stability. *Naunyn-Schmiedeberg's*
370 *Archives of Pharmacology*. 2007. https://doi.org/10.1007/s00210-006-0126-6.

371 (4) Abu-Taha, I. H.; Heijman, J.; Hippe, H. J.; Wolf, N. M.; El-Armouche, A.; Nikolaev, V. O.;
372 Schäfer, M.; Würtz, C. M.; Neef, S.; Voigt, N.; Baczkó, I.; Varró, A.; Müller, M.; Meder,
373 B.; Katus, H. A.; Spiger, K.; Vettel, C.; Lehmann, L. H.; Backs, J.; Skolnik, E. Y.; Lutz, S.;
374 Dobrev, D.; Wieland, T. Nucleoside Diphosphate Kinase-C Suppresses CAMP Formation
375 in Human Heart Failure. *Circulation* **2017**.
376 https://doi.org/10.1161/CIRCULATIONAHA.116.022852.
377 (5) Moréra, S.; Lacombe, M. L.; Yingwu, X.; Joël Janin, G. L. B. and. X-Ray Structure of
378 Human Nucleoside Diphosphate Kinase B Complexed with GDP at 2 å Resolution.
379 *Structure* **1995**. https://doi.org/10.1016/S0969-2126(01)00268-4.
380 (6) Webb, P. A.; Perisic, O.; Mendola, C. E.; Backer, J. M.; Williams, R. L. The Crystal
381 Structure of a Human Nucleoside Diphosphate Kinase, NM23-H2. *J. Mol. Biol.* **1995**.
382 https://doi.org/10.1006/jmbi.1995.0457.
383 (7) Zaccolo, M. CAMP Signal Transduction in the Heart: Understanding Spatial Control for
384 the Development of Novel Therapeutic Strategies. *British Journal of Pharmacology*. 2009.
385 https://doi.org/10.1111/j.1476-5381.2009.00185.x.
386 (8) Luo, M.; Anderson, M. E. Mechanisms of Altered Ca2+ Handling in Heart Failure. *Circ.*
387 *Res.* **2013**. https://doi.org/10.1161/CIRCRESAHA.113.301651.
388 (9) Hippe, H. J.; Luedde, M.; Lutz, S.; Koehler, H.; Eschenhagen, T.; Frey, N.; Katus, H. A.;
389 Wieland, T.; Niroomand, F. Regulation of Cardiac CAMP Synthesis and Contractility by
390 Nucleoside Diphosphate Kinase B/G Protein Bγ Dimer Complexes. *Circ. Res.* **2007**.
391 https://doi.org/10.1161/01.RES.0000264058.28808.cc.
392 (10) Gilman, A. G. G Proteins: Transducers of Receptor-Generated Signals. *Annual review of*
393 *biochemistry*. 1987. https://doi.org/10.1146/annurev.bi.56.070187.003151.

394 (11) Cabrera-Vera, T. M.; Vanhauwe, J.; Thomas, T. O.; Medkova, M.; Preininger, A.; Mazzoni,
395 M. R.; Hamm, H. E. Insights into G Protein Structure, Function, and Regulation. *Endocrine*
396 *Reviews*. 2003. https://doi.org/10.1210/er.2000-0026.
397 (12) Sun, X.; Liu, Z.; Welsher, K.; Robinson, J. T.; Goodwin, A.; Zaric, S.; Dai, H. Nano-
398 Graphene Oxide for Cellular Imaging and Drug Delivery. *Nano Res.* **2008**.
399 https://doi.org/10.1007/s12274-008-8021-8.
400 (13) Sun, X.; Feng, Z.; Hou, T.; Li, Y. Mechanism of Graphene Oxide as an Enzyme Inhibitor
401 from Molecular Dynamics Simulations. *ACS Appl. Mater. Interfaces* **2014**.
402 https://doi.org/10.1021/am500167c.
403 (14) Kim, J.; Cote, L. J.; Kim, F.; Yuan, W.; Shull, K. R.; Huang, J. Graphene Oxide Sheets at
404 Interfaces. *J. Am. Chem. Soc.* **2010**. https://doi.org/10.1021/ja102777p.
405 (15) Ray, A.; Macwan, I.; Singh, S.; Silwal, S.; Patra, P. A Computational Approach for
406 Understanding the Interactions between Graphene Oxide and Nucleoside Diphosphate
407 Kinase with Implications for Heart Failure. *Nanomaterials* **2018**, *8* (2), 57.
408 https://doi.org/10.3390/nano8020057.
409 (16) Humphrey, W.; Dalke, A.; Schulten, K. VMD: Visual Molecular Dynamics. *J. Mol. Graph.*
410 **1996**. https://doi.org/10.1016/0263-7855(96)00018-5.
411 (17) Berman, H. M.; Westbrook, J.; Feng, Z.; Gilliland, G.; Bhat, T. N.; Weissig, H.; Shindyalov,
412 I. N.; Bourne, P. E. The Protein Data Bank. *Nucleic Acids Research*. 2000.
413 https://doi.org/10.1093/nar/28.1.235.
414 (18) MacKerell, A. D.; Bashford, D.; Bellott, M.; Dunbrack, R. L.; Evanseck, J. D.; Field, M. J.;
415 Fischer, S.; Gao, J.; Guo, H.; Ha, S.; Joseph-McCarthy, D.; Kuchnir, L.; Kuczera, K.; Lau,
416 F. T. K.; Mattos, C.; Michnick, S.; Ngo, T.; Nguyen, D. T.; Prodhom, B.; Reiher, W. E.;

417 Roux, B.; Schlenkrich, M.; Smith, J. C.; Stote, R.; Straub, J.; Watanabe, M.; Wiórkiewicz-
418 Kuczera, J.; Yin, D.; Karplus, M. All-Atom Empirical Potential for Molecular Modeling
419 and Dynamics Studies of Proteins. *J. Phys. Chem. B* **1998**.
420 https://doi.org/10.1021/jp973084f.
421 (19) Tang, H.; Liu, D.; Zhao, Y.; Yang, X.; Lu, J.; Cui, F. Molecular Dynamics Study of the
422 Aggregation Process of Graphene Oxide in Water. *J. Phys. Chem. C* **2015**.
423 https://doi.org/10.1021/acs.jpcc.5b07345.
424 (20) Jorgensen, W. L.; Chandrasekhar, J.; Madura, J. D.; Impey, R. W.; Klein, M. L. Comparison
425 of Simple Potential Functions for Simulating Liquid Water. *J. Chem. Phys.* **1983**.
426 https://doi.org/10.1063/1.445869.
427 (21) Phillips, J. C.; Braun, R.; Wang, W.; Gumbart, J.; Tajkhorshid, E.; Villa, E.; Chipot, C.;
428 Skeel, R. D.; Kalé, L.; Schulten, K. Scalable Molecular Dynamics with NAMD. *Journal of*
429 *Computational Chemistry*. 2005. https://doi.org/10.1002/jcc.20289.
430

431 **ASSOCIATED CONTENT**

432 **Supporting Information**

433 Screenshots of the 250ns trajectories of the NDPK-B and NDPK-C interactions in the presence
434 and absence of GO in figures S1 and S2, number of intramolecular hydrogen bonds within
435 NDPK-B and NDPK-C in figure S3, Secondary structure analysis of His118 and its neighboring
436 residues in the presence and absence of GO in figure S4, and Tables ST1 and ST2 showing the
437 intramolecular salt bridges within NDPK-B and NDPK-C.

438 **Data and Software Availability**

Modeling and Simulation software, VMD (Visual Molecular Dynamics) and NAMD (Nanoscale Molecular Dynamics) used in this study are freely available from the Theoretical and Computational Biophysics group at the NIH Center for Macromolecular Modeling and Bioinformatics at the University of Illinois at Urbana-Champaign, http://www.ks.uiuc.edu/Research/vmd/

Atomic coordinate (protein data bank, PDB) files for the two enzymes, NDPK-B and NDPK-C, 1NUE and 1ZS6 were obtained from the database located at Research Collaboratory for Structural Bioinformatics (RCSB), www.rcsb.org.

To create the protein structure files (PSF) and to carry out all – atom simulations, the necessary topology and forcefield parameter files were obtained from the Chemistry at Harvard Macromolecular Mechanics (CHARMM) database located at the MacKerell Lab at the University of Maryland, School of Pharmacy, http://mackerell.umaryland.edu/charmm_ff.shtml. The models for the two systems with and without graphene oxide and the two enzymes NDPK-B and NDPK-C along with the parameter and configuration files are also available as part of the supporting information.

AUTHOR INFORMATION

Corresponding Author

*Tel.: +1-203-254-4000. Fax:+1-203-254-4147. Email: imacwan@fairfield.edu.

Notes

[#]Andrey Zaznaev is presently at Georgia Institute of Technology, Atlanta GA 30332, USA.

The authors declare no competing financial interest.

Author Contributions

The manuscript was written through contributions of all authors. All authors have given approval to the final version of the manuscript.

ACKNOWLEDGMENT

We acknowledge Fairfield University for providing computational resources.

ABBREVIATIONS

NDPK, nucleoside diphosphate kinase; GO, graphene oxide; VMD, Visual Molecular Dynamics; NAMD, NAnoscale Molecular Dynamics.